Nanostructured $LnBaCo_2O_{6-\delta}$ (Ln = Sm, Gd) with layered structure for intermediate temperature solid oxide fuel cell cathodes

Augusto E. Mejía Gómez, Diego G. Lamas, Ana Gabriela Leyva, and Joaquín Sacanell

Citation: AIP Advances **7**, 045214 (2017); doi: 10.1063/1.4981901
View online: http://dx.doi.org/10.1063/1.4981901
View Table of Contents: http://aip.scitation.org/toc/adv/7/4
Published by the American Institute of Physics

Nanostructured $LnBaCo_2O_{6-\delta}$ (Ln = Sm, Gd) with layered structure for intermediate temperature solid oxide fuel cell cathodes

Augusto E. Mejía Gómez,[1,2] Diego G. Lamas,[1,2,3] Ana Gabriela Leyva,[2,3] and Joaquín Sacanell[1,2,a]

[1]*CONICET, Godoy Cruz 2290, Ciudad Autónoma de Buenos Aires (1425), Argentina*
[2]*Departamento Física de la Materia Condensada, Centro Atómico Constituyentes, Comisión Nacional de Energía Atómica, Ave. Gral. Paz 1499, San Martín 1650, Provincia de Buenos Aires, Argentina*
[3]*Universidad Nacional de Gral. San Martín, Escuela de Ciencia y Tecnología, Campus Miguelete, 25 de Mayo y Francia, San Martín 1650, Provincia de Buenos Aires, Argentina*

(Received 22 November 2016; accepted 9 April 2017; published online 24 April 2017)

In this work, we present the combination of two characteristics that are beneficial for solid oxide fuel cell (SOFC) cathodic performance in one material. We developed and evaluated for the first time nanostructured layered perovskites of formulae $LnBaCo_2O_{6-d}$ with Ln = Sm and Gd (SBCO and GBCO, respectively) as SOFC cathodes, finding promising electrochemical properties in the intermediate temperature range. We obtained those nanostructures by using porous templates to confine the chemical reagents in regions of 200-800 nm. The performance of nanostructured SBCO and GBCO cathodes was analyzed by electrochemical impedance spectroscopy technique under different operating conditions using Gd_2O_3-doped CeO_2 as electrolyte. We found that SBCO cathodes displayed lower area-specific resistance than GBCO ones, because bulk diffusion of oxide ions is enhanced in the former. We also found that cathodes synthesized using smaller template pores exhibited better performance. [http://dx.doi.org/10.1063/1.4981901]

Extensive research has been devoted in the last few years to develop novel materials and microstructures for solid oxide fuel cells (SOFC) components to operate in the intermediate temperature (IT) range (500°C - 700°C).[1–7] We have recently shown that the use of nanostructures is beneficial both for electrolytes[8,9] and electrodes.[10–12] In the case of the cathode, we developed nanostructured tubes and rods that show impressively low polarization resistance.[13–16]

Typical SOFC cathodes are made mixed ionic and electronic conductors (MIEC).[17] Among them, layered MIEC perovskites of formula $LnBaCo_2O_{6-\delta}$ (LnBCO, Ln = lanthanide)[18–20] have shown to display fast oxide-ion diffusion due to a reduction of the oxygen bonding strength that leads to the appearance of channels for fast ion motion.[21] The layered ordering of cations or double perovskite structure, characterized by a sequence of atomic layers of Ln followed by a layer of Ba, is due to the large difference between ionic radii of Ba^{2+} ($r_{Ba2+} \sim 1.61$ Å), and Ln^{3+} ions ($r_{Sm3+} \sim 1.24$ Å, $r_{Gd3+} \sim 1.107$ Å, for example). After those early works, numerous studies of LnBCO-based cathodes for IT-SOFCs emerged, dealing with the analysis of different factors relevant for the properties of the cathode, such as electrical conductivity, chemical composition, chemical compatibility, thermal expansion coefficient (TEC) and ASR (see Refs. 22 and 23 and references therein).

Considering those results, it would be desirable to develop cathodes in order to combine both benefits, that related with the layered ordering and to the nanostructured character. However, so far and to the best of our knowledge, no studies have been performed on the study of nanostructured

[a]Author to whom correspondence should be addressed. Electronic mail: sacanell@tandar.cnea.gov.ar

cathodes of LnBCO double perovskites. The main reason may be due to the inherent difficulty to retain the nanostructure in layered perovskite materials, at the typically high temperatures needed for their synthesis procedure.

In this work we successfully obtained nanostructured LnBCO cathodes, with Ln = Gd and Sm, following a similar procedure developed to obtain nanostructured perovskites of different compositions.[24–26] By that method, we were able to retain both the nanostructured character and the double perovskite structure.

The obtained materials were further evaluated as SOFC cathodes that display excellent electrochemical properties in the IT range. Thus, this work paves the way to develop other nanostructured layered perovskite materials in different research areas.

LnBCO nanostructures used as precursors for the cathodes, were synthesized by a pore-wetting technique described in the supplementary material. These materials were smeared with a brush on both sides of $Ce_{0.8}Gd_{0.2}O_{1.9}$ electrolytes (GDC, Nextech Materials) to fabricate symmetrical [LnBCO/GDC/LnBCO] cells. A layer of GDC powder was previously smeared and sintered in both faces of the electrolytes in order to improve the cathodes adherence. The samples were dried at 50°C in air for about 20 min and sintered 1 h at 1050°C, with a heating and cooling rate of 10°C min^{-1}.

The area-specific resistance (ASR) of the cathodes was determined from electrochemical impedance spectroscopy (EIS) measurements performed in air, in pure oxygen and in a mixture of 95% of N_2 and 5% of O_2.

X-ray power diffraction(XPD) data for the LnBCO powders treated at 1050°C are shown in Figure 1. We used the following nomenclature: Cathodes made with $SmBaCo_2O_6$ and templates of 200 nm and 800 nm were labelled as SBCO2 and SBCO8, respectively. Similarly, cathodes made with

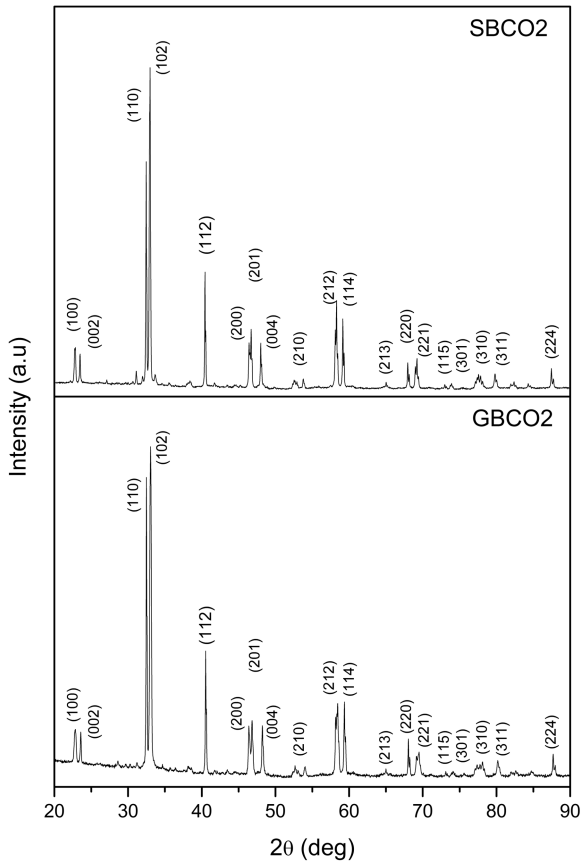

FIG. 1. X-ray diffraction patterns for the samples SBCO2 and GBCO2 treated at 1050°C. Data corresponds to single phase samples with orthorhombic crystal structure of *Pmmm* space group. Only in the case of SBCO2 sample, the presence of $BaCoO_{2+\delta}$ impurity was detected (see text).

TABLE I. Crystallographic data obtained from X-ray diffraction patterns.

	Space Group	Template pore size (nm)	a(Å)	b(Å)	c(Å)	d(nm)
$SmBaCo_2O_{6-\delta}$	Pmmm	200 nm	3.8869 (1)	7.8168 (2)	7.5739 (2)	41
		800 nm	3.8886 (2)	7.8246 (4)	7.5688 (4)	42
$GdBaCo_2O_{6-\delta}$	Pmmm	200 nm	3.8781 (2)	7.8180 (3)	7.5414 (3)	36
		800 nm	3.8789 (3)	7.8196 (5)	7.5419 (5)	40

$GbBaCo_2O_{6-\delta}$ were labeled as GBCO2 and GBCO8. We show the data for samples obtained with templates of 200 nm of diameter, diffractograms corresponding to cathodes obtained with templates of 800 nm present the same crystal structure (see supplementary material). Single phase samples with orthorhombic crystal structure (*Pmmm* space group) were obtained for both compositions and for both template pore size studied in this work: 200 nm and 800 nm. Only in the case of sample SBCO2, we detected a small content of $BaCoO_{2+\delta}$ impurity (of about 2 wt.%, as determined by Rietveld analysis), which provokes a small variation of the cell parameters but did not affect the electrochemical performance, as it will be shown below. Our XPD patterns are consistent with those presented in Reference 27 for Ln: Gd and Ref. 28 for Ln: Sm, indicating that both compounds present an ordered layered crystal structure. In Table I we present the data obtained from XPD data analysis. By analyzing the broadening of Bragg peaks, the average crystallite size was obtained using the Scherrer equation in all cases (see Table I). This is an important result because, to the best of our knowledge, the electrochemical properties of nanostructured layered LnBCO have not been reported in the literature before. Nominal compositions were verified within experimental errors by energy dispersive spectroscopy (EDS).

Field-emission scanning electron microscopy (FE-SEM) micrographs of the plane view of the GBCO2 and GBCO8 cathodes are shown in Figure 2. All cathodes are highly porous, but no signal

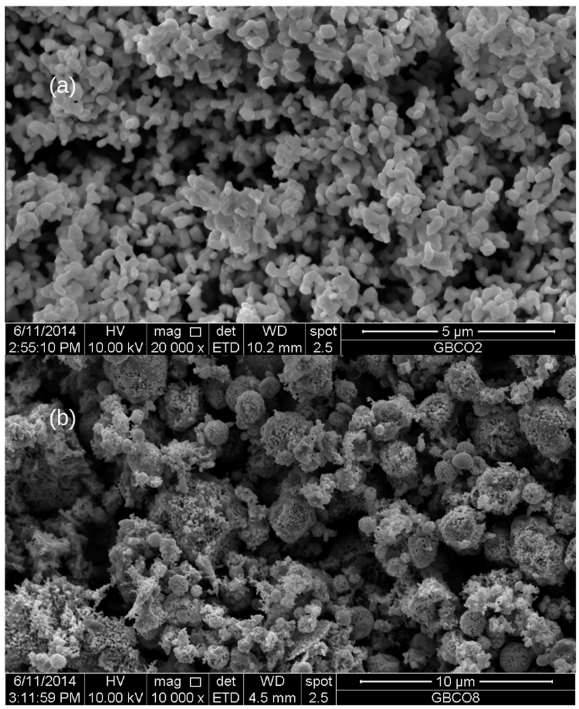

FIG. 2. FE-SEM micrographs of (a) the GBCO2 cathode and (b) the GBCO8 cathode. All cathodes are highly porous. Cathodes made using templates of 200 nm pores are mainly formed by agglomerated nanoparticles with no particular symmetry while cathodes made with templates of 800 nm pores are formed by nanoparticles agglomerated in "sphere-like" structures of micrometric scale.

of a tubular nor filamentary structure is observed, in contrast with previously observed results of other compositions.[13,14] We show micrographs corresponding to $GbBaCo_2O_6$ because both cathodes display similar characteristics, a complete set of pictures of the cathodes can be found on the supplementary material. The BET specific surface area of the precursors (previous to the deposition of the cathode) was 48 and 56 m^2/g for GBCO2 and SBCO2 respectively, while for GBCO8 and SBCO8 we obtained values around 40 m^2/g.

Our cathodes are mainly formed by agglomerated particles of 193±20 nm (SBCO2), 141±29 nm (SBCO8), 122±18 nm (GBCO2) and 99±10 nm (GBCO8) mean diameter. Histograms used to obtain the previous results are presented in the supplementary material. The smaller diameter of the particles in the cathodes obtained from templates of 800 nm (as compared with those of the same composition but using templates of 200 nm), is likely to be related to the small degree of agglomeration resulting in a larger confinement volume of the reactants.

Also, cathodes made with templates of 800 nm display two scales of porosity, they are porous both at the meso- and nanoscales. The former is due to the pore former of the ink vehicle and the latter being a result of the confinement performed by the templates. As a counterpart, particles of that porous structure seems to be weakly connected, giving rise to less percolative paths along the surface of the cathode.

The particles are distributed on larger structures which are reminiscent to porous spheres (for SBCO they are slightly distorted, see supplementary material). Those structures are the result of having used solutions of low concentration to avoid precipitation of the reagents, in relatively large template pores. In the SBCO8 cathode, larger particles of around 3μm can be observed (see supplementary material) which are the GDC powder that was added to improve adherence, as verified by EDS. The presence of those platelets does not seem to have a major influence on the electrochemical behavior of SBCO8, as we will be shown below, because it follows a similar trend as that presented by the other samples.

The adherence of the cathodes was tested by rubbing them gently with a cotton swab and was found to be excellent. We have also verified that the cathodes did not detach after performing several measurement cycles.

The EIS spectra (in air, at 700°C and zero bias) of GBCO2 and GBCO8 is shown in Figure 3(a), while the corresponding spectra of SBCO2 and SBCO8 is shown in Figure 3(b). All materials present promising performance at 700°C, reaching an ASR of 0.4 Ω-cm^2 for the SBCO2 cathode. A significant influence with the diameter of the used precursors has been obtained for the cathode of $GdBaCo_2O_6$, in comparison with the cathode of $SmBaCo_2O_6$, being the latter the one

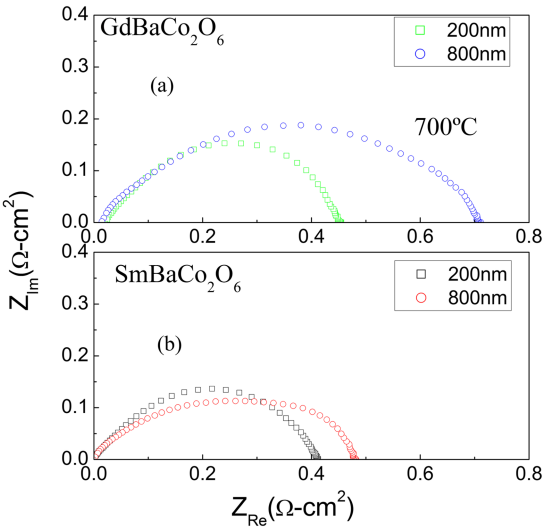

FIG. 3. Electrochemical impedance spectroscopy data at 700°C for (a) GBCO2, GBCO8, (b) SBCO2 and SBCO8. The diameter of the used precursors has much significant influence in Gd-based cathodes than in Sm ones, but the latter displays the lowest ASR. The lowest ASR of each composition is obtained for the precursors synthesized in templates of smaller pores.

displaying the lowest ASR. The lowest ASR of each composition is obtained for the precursors synthesized in templates of smaller pores.

In Figure 4 we show the Arrhenius plot of the ASR for all cases. We can see that almost all cathodes reach ASR values lower than 1 Ω.cm^2 above 650°C and of the order of 0.5 Ω-cm^2 at 700°C. In the inset we sketch the values of ASR as a function of each sample to analyze the influence of composition and nanostructure. The ORR activity can be assumed as proportional to 1/ASR.[29] In this sense, at high temperatures cathodes SBCO2 and GBCO2 are clearly those displaying the highest ORR activity, showing that the microstructure dominates the behavior of the cathode. On the other hand, on increasing temperature, composition seems to be much significant, as cathodes made with $SmBaCo_2O_6$ display higher ORR activity than cathodes of $GdBaCo_2O_6$ for fixed microstructure.

We found that the EIS spectra of our cathodes mainly consist two processes. One dominant process at intermediate and large frequencies, corresponding to a finite length Warburg element as it is usual in cathodes with high oxide ion conductivity, in series with a parallel between a resistor (R_1) and a constant phase element(Q_1) at low frequencies. No additional contributions were needed in order to fit the data.

In the supplementary material, we present the dependence of R_W and R_1 with oxygen partial pressure ($p(O_2)$). Data was analyzed using

$$R_i = A.p\,(O_2)^{-n}\ (i = \mathrm{W\ or\ 1}) \tag{1}$$

In equation (1), "*A*" is a constant and "*n*" is a signature of the dominating process that gives rise to each component.[30] For almost all cathodes, the adjustment of R_W yielded a value of *n* of 0.11 to 0.14 (Table S-II of the supplementary material), which is compatible with bulk diffusion of oxide ions. The only exception is GBCO2 in which *n* is 0.24, suggesting a limiting step of oxygen exchange redox reaction on the electrode surface between the adsorbed oxygen and the bulk electrode material.[30]

From the analysis of R_1 (Table S-III of the supplementary material) of SBCO2, SBCO8 and GBCO8, we obtained *n* between 0.57 and 0.67, indicating a complex mechanism with an intermediate value between 0.5 (characterizing a dissociative adsorption-limitingstep) and 1 (indicating a gas-phase diffusion-limiting step), while for GBCO2 the value of 1.02 clearly shows that this component mainly arises from gas-phase diffusionthrough the cathode pores.[30]

The values of the resistive parts of the equivalent circuit obtained by fitting the data at 700°C, are presented in Table II (we present the fitting of the EIS data at different oxygen partial pressures in the supplementary material). In all cases, the resistive part of the Warburg element (R_W) represent the most significant part of the ASR. By the ratio R_W/R_1 we can compare the relative influence of each component. Comparing SBCO2 and SBCO8, with very similar values of R_1, its relative influence is major in SBCO2. This means that SBCO2 has a smaller resistance associated with oxide

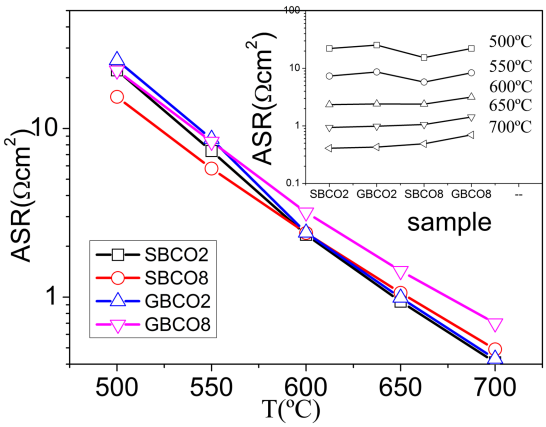

FIG. 4. Area Specific Resistance as a function of temperature. Most cathodes reach lower ASR than 1 Ω.cm^2 above 650°C and of the order of 0.5 Ω -cm$_2$ at 700°C. Inset: ASR as a function of the sample. Standard deviation of the data is smaller than the size of the experimental points.

TABLE II. Resistive parts of the fitting components. R_W (corresponding to intermediate to high frequency the Warburg element) and R_1 (corresponding to the low frequency R_1Q_1 parallel). Standard deviation of R_W and R_1 are 0.01 Ω-cm^2.

	SBCO2	SBCO8	GBCO2	GBCO8
R_W	0.28 Ω-cm^2	0.39 Ω-cm^2	0.41 Ω-cm^2	0.6 Ω-cm^2
R_1	0.14 Ω-cm^2	0.13 Ω-cm^2	0.04 Ω-cm^2	0.14 Ω-cm^2
R_W/R_1	0.5	0.33	~0.1	0.23

ion diffusion than SBCO8. Such comparison is difficult between GBCO2 and GBCO8, because both resistive components differ for those cathodes, however, it is clear that the diffusion resistance (R_W) is smaller in GBCO2 than in GBCO8. For both template pore sizes,we observed that Sm-based cathodes display better performance.

In summary, we obtained nanostructured layered perovskites of $SmBaCo_2O_6$ and $GbBaCo_2O_{6-\delta}$ by a very simple procedure and attached to an electrolyte retaining its original nanostructured character. This is the first report of the evaluation of nanostructured materials that present a layered perovskite structure, as cathodes of SOFC.

Our cathodes are highly porous as it is clear from FE-SEM images. This is probably related with the powders used as precursors for the cathodes, as reactants are confined in disconnected template pores of sub-micrometric diameter. Thus, the growth of the particles is constrained and also the as prepared power is highly dissaglomerated.[13,14]

All cathodes display very low ASR in the IT range, as compared with cathodes of similar compositions,[23] moreover taking into account that they were simply smeared with a brush for deposition. Our results show that cathodes prepared using templates of smaller diameter display an enhanced performance. The main reason for this behavior is the higher degree of disagglomeration of the particles that compose the cathode. Besides, our results show that Sm-based cathodes display better performance than Gd-based ones in agreement with previous reports.[22] The main contribution to ASR is bulk diffusion of oxide ions, with a minor low frequency contribution ascribed to dissociative adsorption and gas phase diffusion.

Besides the promising results in the area of IT-SOFCs, the successful synthesis of nanostructured layered perovskites paves the way for their use in other applications such as magnetoresistive materials or materials for solar cells.

SUPPLEMENTARY MATERIAL

See supplementary material for a detailed Materials and Methods section, a detailed description of the synthesis procedure, additional FE-SEM images and complementary data regarding the EIS analysis.

ACKNOWLEDGMENTS

The present work was partially supported by Agencia Nacional de Promoción Científica y Tecnológica (Argentina, PICT 2011 No. 1948 and PICT 2015 No. 3411) and CONICET (Argentina, PIP 000362-2011). The authors thank Dr. Valeria Fuertes (CONICET-UNC, Argentina) for useful comments on XPD analysis.

[1] A. Esquirol, N. Brandon, J. A. Kilner, and M. Mogensen, J. Electrochem. Soc. **151**, A1847–A1855 (2004).
[2] Z. Shao and S. M. Halle, Nature **431**, 170–173 (2004).
[3] B. C. H. Steele, K. M. Hori, and S. Uchino, Solis State Ionics **135**, 445–450 (2000).
[4] J. B. Goodenough, Annual Review of Materials Research **33**, 91–128 (2003).
[5] A. J. Jacobson, Chemistry of Materials **22**, 660–674 (2010).
[6] D. J. L. Brett, A. Atkinson, N. P. Brandon, and S. J. Skinner, Chemical Society Reviews **37**, 1568–1578 (2008).
[7] V. Dusastre and J. A. Kilner, Solid State Ionics **126**, 163–174 (1999).
[8] M. G. Bellino, D. G. Lamas, and N. E. Walsöe De Reca, Advanced Materials **18**, 3005–3009 (2006).
[9] P. M. Abdala, G. S. Custo, and D. G. J. Lamas, Power Sources **195**, 3402–3406 (2010).
[10] S. Larrondo, M. A. Vidal, B. Irigoyen, A. F. Craievich, D. G. Lamas, I. O. Fábregas, G. E. Lascalea, N. E. W. De Reca, and N. Amadeo, Catalysis Today **107-108**, 53–59 (2005).

[11] S. A. Larrondo, A. Kodjaian, I. Fábregas, M. G. Zimicz, D. G. Lamas, B. E. Walsöe de Reca, and N. E. Amadeo, International Journal of Hydrogen Energy **33**, 3607–3613 (2008).
[12] L. M. Acuña, J. Peña-Martínez, D. Marrero-López, R. O. Fuentes, P. Nuñez, and D. G. J. Lamas, Power Sources **196**, 9276–9283 (2011).
[13] M. G. Augusto, J. Sacanell, A. G. Leyva, and D. G. Lamas, Ceramics International **42**, 3145–3153 (2016).
[14] J. Sacanell, A. Gabriela Leyva, M. G. Bellino, and D. G. Lamas, J. Power Sources **195**, 1786–1792 (2010).
[15] M. G. Bellino, J. G. Sacanell, D. G. Lamas, A. G. Leyva, and N. E. Walsöe de Reca, ECS Transactions - Solid Oxide Fuel Cells **7**(1), 1299 (2007).
[16] M. G. Bellino, J. G. Sacanell, D. G. Lamas, A. G. Leyva, and N. E. Walsöe de Reca, JACS **129**(11), 3066–3067 (2007).
[17] S. B. Adler, Chem. Rev. **104**(10), 4791–4843 (2004).
[18] J.-H. Kim and A. Manthiram, J. Electrochem, Soc. **155**(4), B385–B390 (2008).
[19] A. Tarancón, S. Skinner, R. Chater, F. Hernández-Ramírez, and J. Kilner, J. Mater. Chem. **17**, 3175–3181 (2007).
[20] J.-H. Kim, L. Mogni, F. Prado, A. Caneiro, J. A. Alonso, and A. J. Manthiram, Electrochem. Soc. **156**, B1376–B1382 (2009).
[21] A. A. Taskin, A. N. Lavrov, and Y. Ando, Appl. Phys. Lett. **86**, 91910 (2005).
[22] R. Pelosato, G. Cordaro, D. Stucchi, C. Cristiani, and G. Dotelli, J. Power Sources **298**, 46–67 (2015).
[23] J.-H. Kim and A. Manthiram, J. Mater. Chem. **A3**, 24195–24210 (2015).
[24] A. G. Leyva, P. Stoliar, M. Rosenbusch, V. Lorenzo, P. Levy, C. Albonetti, M. Cavallini, F. Biscarini, H. E. Troiani, J. Curiale, and R. D. Sanchez, J. Solid State Chem. **177**, 3949–3953 (2004).
[25] P. Levy, A. G. Leyva, H. E. Troiani, and R. D. Sanchez, Appl. Phys. Lett. **83**, 5247–5249 (2003).
[26] J. Sacanell, M. G. Bellino, D. G. Lamas, and A. G. Leyva, Physica B **398**, 341–343 (2007).
[27] L. Lo Presti, M. Allieta, M. Scavini, P. Ghigna, L. Loconte, V. Scagnoli, and M. Brunelli, Phys. Rev. B **84**, 104107 (2011).
[28] L. Y. Gavrilova, T. V. Aksenova, N. E. Volkova, A. S. Podzorova, and V. A. Cherepanov, J. Solid State Chem. **184**, 2083–2087 (2011).
[29] Y.-L. Lee, J. Kleis, J. Rossmeisl, Y. Shao-Horn, and D. Morgan, Energy Environ. Sci. **4**, 3966 (2011).
[30] A. Ringuedé and J. Fouletier, Solid State Ionics **139**, 167–177 (2001).